

# Let Language Constrain Geometry:

## Vision–Language Models as Semantic and Spatial Critics for 3D Generation

Weimin Bai<sup>1†</sup>, Yubo Li<sup>1†</sup>, Weijian Luo<sup>2</sup>, Zeqiang Lai<sup>3</sup>, Yequan Wang<sup>4</sup>, Wenzheng Chen<sup>1‡</sup>, He Sun<sup>1‡</sup>

1. Peking University 2. Xiaohongshu Inc 3. MMLab, CUHK 4. BAAI, Beijing

<https://ai4scientificimaging.org/vlm3d>

### Abstract

*Text-to-3D generation has advanced rapidly, yet state-of-the-art models, encompassing both optimization-based and feed-forward architectures, still face two fundamental limitations. First, they struggle with coarse semantic alignment, often failing to capture fine-grained prompt details. Second, they lack robust 3D spatial understanding, leading to geometric inconsistencies and catastrophic failures in part assembly and spatial relationships. To address these challenges, we propose VLM3D, a general framework that repurposes large vision-language models (VLMs) as powerful, differentiable semantic and spatial critics. Our core contribution is a dual-query critic signal derived from the VLM’s “Yes/No” log-odds, which assesses both semantic fidelity and geometric coherence. We demonstrate the generality of this guidance signal across two distinct paradigms: (1) As a reward objective for optimization-based pipelines, VLM3D significantly outperforms existing methods on standard benchmarks. (2) As a test-time guidance module for feed-forward pipelines, it actively steers the iterative sampling process of SOTA native 3D models to correct severe spatial errors. VLM3D establishes a principled and generalizable path to inject the VLM’s rich, language-grounded understanding of both semantics and space into diverse 3D generative pipelines.*

### 1. Introduction

Creating 3D content from natural language descriptions has drawn significant attention [12, 26, 34, 50, 51]. Recent models, encompassing both optimization-based paradigms [26] and high-speed feed-forward architectures [12, 50, 51], have achieved impressive results. However, state-of-the-art models across both paradigms still face two fundamental limitations. First, they struggle with coarse semantic alignment, often failing to capture fine-grained prompt details or complex interactions. For instance, given a detailed description of the “Embracing Peace” monument, even the powerful MVDream

baseline omits one of the two figures entirely (see Figure 1 top). Second, they lack robust 3D spatial understanding. For instance, SOTA feed-forward models [12, 50, 51] can fail in part assembly and spatial relationships, generating nonsensical, floating collections of parts instead of coherent objects (see Figure 1 bottom). These failures arise from inadequate priors and limited reasoning: optimization-based methods inherit weak semantic grounding and poor spatial awareness from 2D diffusion models, while feed-forward methods are constrained by the limited complexity of 3D training data (often single objects rather than multi-object scenes), leading to poor modeling of 3D structure and compositional semantics. Both ultimately lack a deep understanding of spatial relationships and language.

To address these challenges across paradigms, we propose VLM3D, a 3D generation framework that integrates large vision-language models (VLMs) [1, 3] as powerful, differentiable semantic and spatial critics. Instead of relying on the weak semantic grounding of CLIP-style encoders [29, 48] or the 2D-centric priors of diffusion models [32, 34], we leverage the VLM’s rich, language-grounded understanding of both fine-grained semantics and complex 3D spatial relationships [6, 8, 49].

Our core contribution is a dual-query VLM-based critic signal that simultaneously optimizes the 3D representation for both semantic fidelity and spatial/geometric coherence. Specifically, our framework tasks the VLM to act as a dual-objective reward model. It evaluates the multi-view renderings against a structured query comprising two distinct criteria: (1) Content Match: assessing correspondence to the semantic description, and (2) Geometric Quality: assessing whether the object is geometrically sound and consistent across views. The VLM is constrained to output only *Yes* or *No*; we then design our differentiable VLM reward based on the extracted log-odds. Backpropagating this signal provides a direct semantically-grounded and spatially-aware gradient for optimizing the 3D representation.

We demonstrate the generality of the proposed VLM-based critic by applying it across two distinct paradigms:

<sup>†</sup>Equal Contributions. <sup>‡</sup>Corresponding authors.

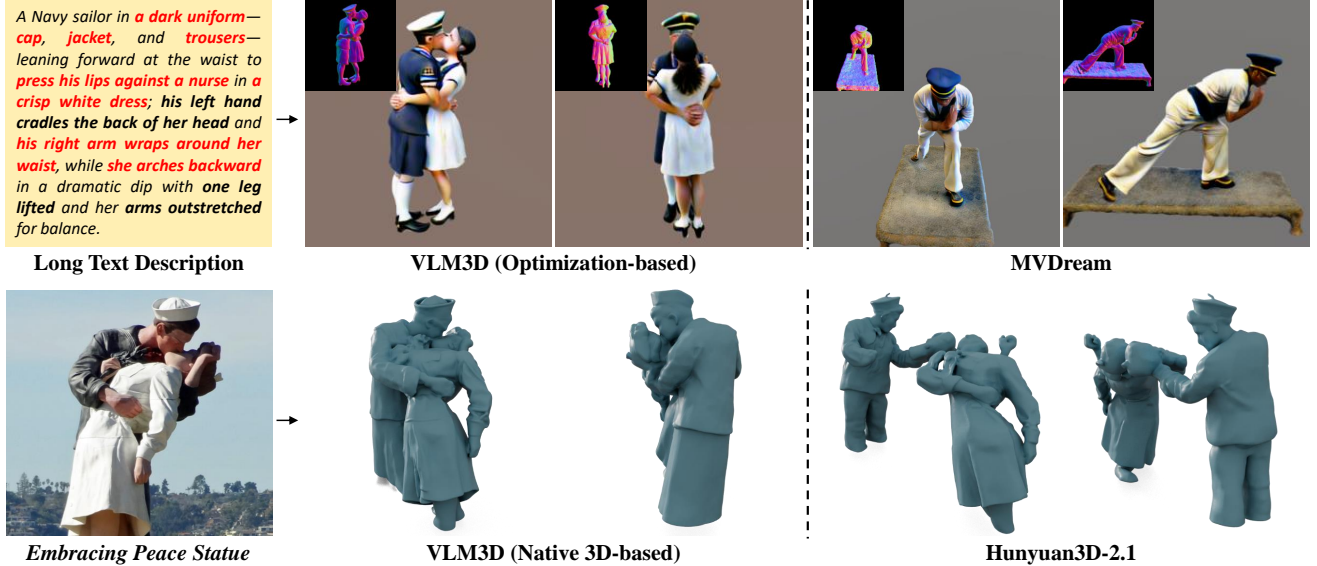


Figure 1. **Reproducing the “Embracing Peace” Statue with VLM3D.** We challenge VLM3D’s dual paradigms with San Diego’s iconic monument. **Top (Optimization-based):** Given a long text description, baseline MVDream [34] suffers a catastrophic semantic failure, omitting the nurse entirely. Our VLM3D critic successfully recovers both figures and their signature pose. Key details are highlighted in red. **Bottom (Feed-forward model-based):** Comparing to the statue’s reference image, baseline Hunyuan3D [12] generates a distorted, spatially incoherent mesh. Our VLM3D substantially corrects these spatial failures and produces a more geometrically plausible 3D asset.

- **Score Distillation Sampling:** We integrate VLM3D into an optimization-based pipeline SDS [26, 34]. On standard benchmarks like GPTEval3D [43], VLM3D significantly outperforms existing methods in semantic accuracy and 3D plausibility. It successfully captures complex semantics (Fig. 1) and resolves geometric inconsistencies (Fig. 6).
- **Feed-forward Models:** We show that VLM3D can be deeply integrated into the iterative sampling loop of SOTA native 3D feed-forward models [12, 51]. As shown in Fig. 4, our test-time guidance approach effectively corrects severe geometric and part-assembly errors, producing coherent 3D assets where the original models failed.

To the best of our knowledge, VLM3D makes the first attempt to establish a principled and generalizable path to inject the VLM’s rich, language-grounded understanding of both semantics and space into both optimization-based and feed-forward-based 3D generative pipelines.

## 2. Related Works

Our work builds upon the intersection of two major paradigms in text-to-3D generation and the rapid advancements in vision-language models.

### 2.1. Optimization-based Text-to-3D Generation

The first dominant paradigm leverages 2D diffusion priors [9, 32] to guide the per-scene optimization of a 3D representation. SDS [26] pioneered this by using the gradients from a pre-trained 2D diffusion model to optimize a Neural Radiance Field (NeRF) [22]. This distillation process

enables plausible 3D asset creation from text without 3D data [26].

Subsequent methods improved this foundation. Magic3D introduced a coarse-to-fine optimization strategy [19]. MV-Dream trained a diffusion model on multi-view data to produce more 3D-consistent priors [34], while ProlificDreamer framed the process as variational inference to improve diversity [41]. Other works have focused on integrating explicit reward models, such as DreamReward, which uses a 3D reward model trained on human feedback [46].

Despite their success, these methods inherit the limitations of their 2D priors. Their guidance signals often lack fine-grained semantic understanding, relying on CLIP-style encoders [28, 30] that struggle with complex prompts. Furthermore, being 2D-native, these priors lack explicit 3D spatial reasoning, leading to view-inconsistencies like the Janus problem [10, 23, 33, 42]. Our work addresses these semantic and spatial gaps with a VLM-based reward.

### 2.2. Feed-Forward Text-to-3D Generation

The second major paradigm is feed-forward models, developed to overcome the slow optimization of SDS. These methods aim to generate 3D assets in a single forward pass, enabling near real-time creation. Early approaches focused on generating explicit representations like point clouds or voxels. More recently, methods like Instant3D [17], LRM [11] and GRM [45] first generate consistent multi-view images and then use a fast reconstruction model to produce NeRF or 3D Gaussian Splatting [14] assets.

Note, recent native 3D diffusion models [12, 50, 51], which we also categorize as feed-forward, require an iterative sampling process to generate the final asset. These SOTA feed-forward models are trained on large-scale 3D datasets to directly output 3D representations from text or images. While extremely efficient, this speed can come at the cost of fidelity and coherence. These challenges are often attributable to the inherent limitations of current 3D training data, which remains relatively scarce and is largely constrained to single objects, lacking complex, multi-object scenes. Consequently, as demonstrated in Fig. 1, these models can exhibit notable limitations in spatial intelligence, such as generating disconnected parts, incomplete geometry, or incorrect spatial relationships. They also struggle with capturing the precise, fine-grained semantic attributes specified in a prompt. This highlights a critical need for a refinement mechanism. Our work positions VLM3D as a general test-time guidance module to address exactly these semantic and spatial failures.

### 2.3. Vision-Language Models

Our solution is powered by modern vision-language models. Early VLMs like CLIP [5, 13, 29], while foundational, were trained with contrastive learning. This discriminative objective limits their generative flexibility [18, 31, 47] and, crucially, their fine-grained spatial reasoning capabilities [6, 24, 27, 39].

Modern large VLMs extend this foundation by integrating a powerful autoregressive language model with a visual encoder in an end-to-end, generative framework. Methods like BLIP-2 [16] and MiniGPT-4 [53] leverage lightweight query modules or adapters to bridge frozen vision and language backbones [16, 53], then fine-tune on multimodal instruction data to support open-ended tasks such as image captioning, visual question answering, dense grounding, and dialogue [20]. More recently, models such as LLaVA [20, 37] and Qwen-VL [3] have demonstrated advanced spatial grounding capabilities—localizing objects, understanding complex relations, and reasoning over multi-object scenes—while retaining strong semantic alignment. Notably, these models incorporate advanced vision modules—for example, Qwen2.5-VL employs dynamic resolution processing to natively handle variable-size images and absolute time encoding for precise long-range video reasoning—further enhancing their spatiotemporal understanding [3, 40]. Because these VLMs provide language-grounded similarity measures and implicitly encode spatial relationships, they serve as ideal reward functions within text-to-3D generation pipelines [12, 26, 41, 50, 51].

## 3. Preliminary

**2D Text-to-Image Diffusion Models** Diffusion models [9, 35, 36] define a forward-time SDE that gradually injects

noise into a data sample and a corresponding reverse-time SDE that removes noise to generate samples. Concretely, for an image  $\mathbf{x}_0$  conditioned on text prompt  $y$  (i.e.,  $\mathbf{x}_0 \sim p_{\text{data}}(\cdot | y)$ ), the forward SDE is

$$d\mathbf{x}_t = f(\mathbf{x}_t, t) dt + g(t) d\mathbf{w}_t, \quad (1)$$

and the reverse-time SDE is

$$d\mathbf{x}_t = [f(\mathbf{x}_t, t) - g(t)^2 \nabla_{\mathbf{x}_t} \log p_t(\mathbf{x}_t | y)] dt + g(t) d\bar{\mathbf{w}}_t, \quad (2)$$

where  $t \in [0, T]$ ,  $f$  is the drift,  $g$  the diffusion coefficient,  $\mathbf{w}_t$  and  $\bar{\mathbf{w}}_t$  are forward and reverse Wiener processes, and  $p_t(\cdot | y)$  is the marginal at time  $t$ . A neural network  $s_\phi(\mathbf{x}, y, t) \approx \nabla_{\mathbf{x}} \log p_t(\mathbf{x} | y)$  is trained via denoising score matching to approximate the score function:

$$\mathcal{L}_{\text{DSM}} = \mathbb{E}_{t, \mathbf{x}_0, \epsilon} \left[ \lambda(t) \left\| s_\phi(\mathbf{x}_t, y, t) + \frac{\epsilon}{\sigma(t)} \right\|^2 \right], \quad (3)$$

with  $\mathbf{x}_t = \mathbf{x}_0 + \sigma(t) \epsilon$  and  $\epsilon \sim \mathcal{N}(\mathbf{0}, \mathbf{I})$ .

**Optimization-based Generation** One of the most widely used optimization-based methods for 3D generation is SDS [26]. It repurposes a pretrained 2D score network  $s_\phi$  [32, 34] to optimize 3D object parameters  $\theta$  (e.g., NeRF weights). Let  $I(\theta, v) = \text{Render}(\theta, v)$  be the image produced by a differentiable renderer parameterized by  $\theta$  from viewpoint  $v$ . The SDS loss provides a gradient,  $\nabla_\theta \mathcal{L}_{\text{SDS}}$ , which steers  $\theta$  over thousands of iterations to match the 2D diffusion prior.

$$\nabla_\theta \mathcal{L}_{\text{SDS}} \approx \mathbb{E}_{t, \epsilon} \left[ w(t) \left( s_\phi(\mathbf{x}_t, y, t) + \frac{\epsilon}{\sigma(t)} \right) \frac{\partial I(\theta, v)}{\partial \theta} \right]. \quad (4)$$

This per-object optimization process, while slow, can produce high-fidelity assets. Our VLM3D reward ( $r_{\text{VLM}}$ ) can be integrated as a powerful guidance signal within this iterative optimization framework.

**Feed-Forward Generation** Feed-forward methods produce a 3D asset efficiently, comprising two major variants:

- **Hybrid Feed-Forward:** These methods first generate consistent multi-view 2D images via a diffusion model, and then apply a deterministic reconstruction algorithm to obtain the final 3D shape [11, 17, 45].
- **Native 3D Feed-Forward:** SOTA models like Hunyuan3D [12, 51] and CLAY [50] are true 3D generative models that operate directly on a 3D latent representation (e.g., defined by an encoder  $\mathcal{E}^*$  and decoder  $\mathcal{D}^*$ ). In this case, a *single feed-forward generation* requires multiple internal iterative steps of the core network (e.g., a DiT [25]) to solve the reverse SDE and sample the final 3D asset.

Crucially, this iterative *inference* process is distinct from the iterative *optimization* process of SDS (which runs for

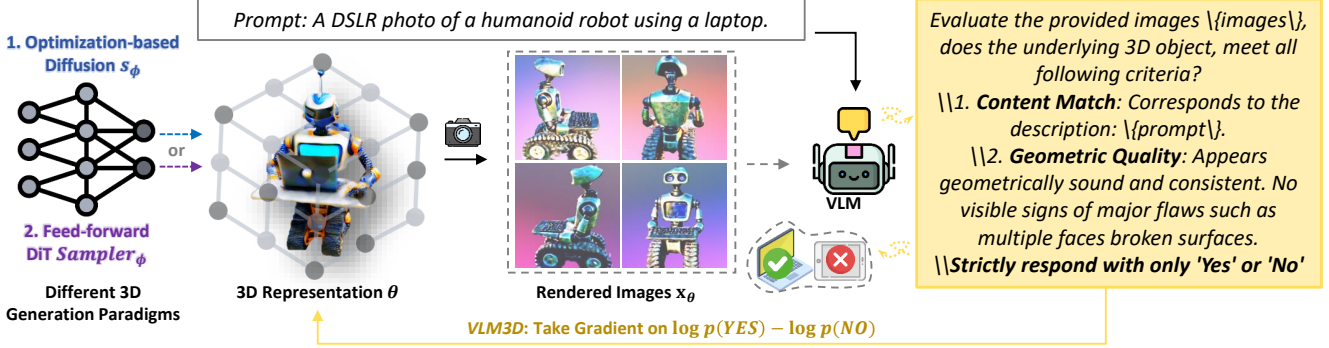


Figure 2. **Overview of VLM3D as a General Critic Framework.** Our core contribution, a differentiable dual-query  $r_{VLM}$ , acts as a versatile critic for 3D generation. It can be applied in two distinct paradigms: (1) As a Reward Objective: It is integrated into optimization-based pipelines (e.g., SDS [26]), replacing 2D priors with rich semantic and spatial reward. (2) As a Test-Time Guidance Module: It is used to guide the 3D assets sampling process of the native 3D models (e.g., Hunyuan3D [12]), correcting their semantic and spatial errors.

thousands of steps). As discussed in Sec. 2.2, while these efficient models often produce assets with sharp shapes and rich geometric details, their reliance on limited training data can lead to weaknesses in fine-grained semantic understanding and complex multi-object spatial reasoning. This makes them prime candidates for our test-time guidance module.

## 4. Method

We now describe our proposed framework, VLM3D, which provides a general, differentiable semantic and spatial critic from a pre-trained VLM. In Sec. 4.1 and Sec. 4.2, we detail the core of our framework: the definition of our differentiable VLM signal ( $r_{VLM}$ ) and the dual-query design that enables it to act as a semantic and spatial critic. Finally, in Sec. 4.3, we describe how this critic is integrated into two distinct paradigms: (1) optimization-based pipelines [26, 34], and (2) SOTA native 3D feed-forward models [12, 51].

### 4.1. Vision-Language Model as an Explicit Semantic and Spatial Critic

We leverage a pre-trained VLM to provide a fully differentiable critic that measures both semantic fidelity and geometric consistency across multi-view renderings. Concretely, let the set of  $N$  images rendered from our 3D representation parameters  $\theta$  under viewpoints  $v_i$

$$\mathcal{X} = \{x_i\}_{i=1}^N = \{I(\theta, v_1), \dots, I(\theta, v_N)\} \quad (5)$$

and the user’s text prompt  $y$  be the two inputs to the large VLM, we constrain the VLM function  $Q(\cdot, \cdot)$ , via carefully engineered queries, to output exclusively “Yes” or “No”,

$$Q(y, \mathcal{X}) \mapsto \{\text{Yes}, \text{No}\}. \quad (6)$$

Then we extract the final “Yes” and “No” logits of the VLM’s binary-classification head,  $z_{\text{yes}}$  and  $z_{\text{no}}$ . The corresponding

probabilities are

$$P(\text{Yes} | y, \mathcal{X}) = \frac{e^{z_{\text{yes}}}}{e^{z_{\text{yes}}} + e^{z_{\text{no}}}}, \quad P(\text{No} | y, \mathcal{X}) = \frac{e^{z_{\text{no}}}}{e^{z_{\text{yes}}} + e^{z_{\text{no}}}}. \quad (7)$$

We define the VLM critic based on the log-odds:

$$r_{VLM} = \log P(\text{Yes} | y, \mathcal{X}) - \log P(\text{No} | y, \mathcal{X}) = z_{\text{yes}} - z_{\text{no}}. \quad (8)$$

The entire mapping  $\theta \rightarrow \mathcal{X} \rightarrow r_{VLM}$  is differentiable, so we can backpropagate through the VLM to update  $\theta$  directly.

### 4.2. VLM Dual-Query Design

Our full query  $y$  to the VLM is structured as follows:

*“Carefully evaluate the provided images, which show multiple views of a single 3D object. Does the underlying 3D object, considering all views together, meet all of the following criteria simultaneously?”*

1. *Content Match: The object corresponds to the description: {text description}.*
2. *Geometric Quality: Based on all views combined, the object appears geometrically sound and consistent. There are no visible signs of major flaws such as multiple faces on one part (Janus-faced issue), broken surfaces, intersecting geometry, or highly unrealistic polygonal facets when considering the object from these different perspectives.*

*Strictly respond with only ‘Yes’ or ‘No’.”*

Our framework tasks the VLM to act as a dual-objective critic. It evaluates the multi-view renderings against this structured query comprising two distinct criteria: (1) Content Match (assessing semantic fidelity) and (2) Geometric Quality (assessing spatial coherence). This dual-query setup ensures that the critic in Eq. 8 captures both semantic alignment and spatial coherence.

### 4.3. Application Frameworks

Our general  $r_{VLM}$  reward can be flexibly integrated into different 3D generation paradigms. We demonstrate its ver-

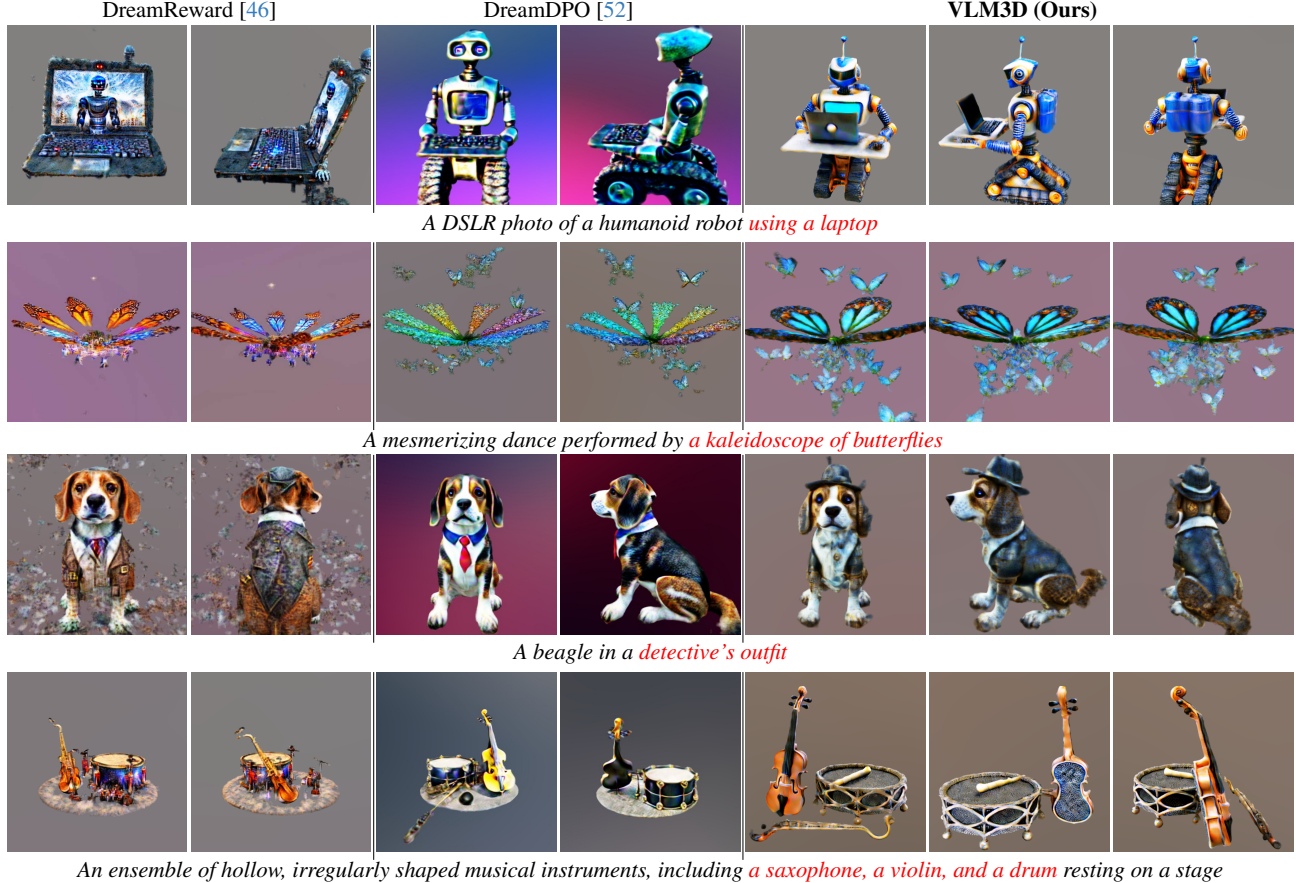


Figure 3. **Comparison of VLM3D with optimization-based baselines.** VLM3D outperforms these methods [46, 52] in semantic fidelity while retaining high perceptual quality. Although baseline methods achieve good texture and detail—via differentiable preference rewards or non-differentiable optimization—they often miss fine-grained concepts (highlighted in red) that VLM3D captures accurately.

satility in two primary frameworks.

#### 4.3.1. Reward for Optimization-based Pipelines

In the first framework,  $r_{\text{VLM}}$  serves as the key reward objective within an optimization-based pipeline. The full training objective combines the VLM reward with the standard SDS loss [26], which provides texture and style priors. Specifically, we minimize:

$$\mathcal{L}_{\text{total}} = \mathcal{L}_{\text{SDS}} - \lambda_{\text{VLM}} r_{\text{VLM}}. \quad (9)$$

where  $\lambda_{\text{VLM}}$  is the balancing factor.

We adopt a dynamic schedule for  $\lambda_{\text{VLM}}$  during training. Initially, we set  $\lambda_{\text{VLM}}$  high to enforce strong semantic and geometric constraints, ensuring the coarse shape aligns with the prompt. We then gradually decay  $\lambda_{\text{VLM}}$  so that the SDS loss predominates, refining textures and fine details. This annealing schedule accelerates convergence and yields high-fidelity, semantically precise assets.

#### 4.3.2. Test-Time Guidance for Feed-Forward Models

In the second framework,  $r_{\text{VLM}}$  is used as a test-time guidance signal, deeply integrated into the iterative sampling

process of pre-trained, native 3D feed-forward models (like the DiT-based Hunyuan3D [12]). At each step  $t$  of the  $T$ -step denoising process (Sec. 3), our method computes the VLM guidance gradient  $\nabla_{\mathbf{z}_t} r_{\text{VLM}}$  based on a differentiable rendering of the current prediction. This gradient is then used to modify the sampling direction, conceptually:

$$\mathbf{z}_{t-1} = \text{Sampler}(\mathbf{z}_t, t) + \lambda_{\text{TTG}} \nabla_{\mathbf{z}_t} r_{\text{VLM}}. \quad (10)$$

This in-process guidance acts as a powerful semantic and spatial critic, steering the generation away from incoherent paths before they solidify. As in [4, 15], this test-time guidance approach requires no model re-training.

## 5. Experiment

We now evaluate VLM3D’s performance, demonstrating its effectiveness and generality across two major 3D generation paradigms. We first present our results integrating  $r_{\text{VLM}}$  into optimization-based pipelines, followed by our results applying  $r_{\text{VLM}}$  as a test-time guidance module to SOTA feed-forward models. We conclude with ablation studies. Additional implementation details and results are provided in the supplementary material.



Figure 4. **Comparison of VLM3D with feed-forward baselines.** We present a qualitative comparison with SOTA native 3D models [12, 50]. Baselines exhibit significant failures, generating incomplete geometry, disconnected parts or distorted shapes. Our VLM3D, integrated as a test-time guidance module to the [12] pipeline, successfully corrects these severe spatial faults and produces coherent 3D assets.

### 5.1. VLM Reward for Optimization-based Pipeline

For this paradigm, we use MVDream [34] as our text-to-image diffusion backbone and Qwen2.5-VL 7B [3] as the VLM reward backbone. The annealing schedule for  $\lambda_{\text{VLM}}$  is detailed in Sec. 4.3.1. All experiments are run on a single NVIDIA A100 GPU with 2.2 hours per 3D asset.

**Setup** We evaluate on the comprehensive GPTEval3D benchmark [44], which contains a diverse set of text prompts. Following this benchmark, we employ GPT-4o-mini to perform pairwise comparisons, calculating Elo ratings that emulate human judgments of text alignment, 3D plausibility, and texture-geometry coherence. We compare against representative score distillation-based methods: DreamFusion [26], DreamGaussian [38], Magic3D [19], ProlificDreamer [41], MVDream [34], DreamReward [46], and DreamDPO [52].

**Quantitative Evaluation on GPTEval3D** Table 1 reports performance of VLM3D against baselines on six metrics: Text–Asset Alignment, 3D Plausibility, Texture Details, Geometry Details, Texture–Geometry Coherence, and Overall

<sup>1</sup>Our metrics differ from those reported in the original DreamReward paper because GPT-4V has been deprecated in GPTEval3D, so we instead use GPT-4o-mini.

Score. VLM3D—which integrates explicit VLM critic with SDS—outperforms all baselines on every metric. In particular, it achieves the top Text–Asset Alignment score, confirming that VLM critic substantially enhances semantic fidelity. It also leads in 3D Plausibility and perceptual quality (both texture and geometry). Overall, VLM3D’s aggregate score surpasses the strongest baseline by a large margin, demonstrating the complementary benefits of combining SDS and VLM-based critic.

**Qualitative Comparison** Fig. 3 shows example 3D assets generated by current SOTA baselines [46, 52] for several prompts. Although these methods boost perceptual quality, they still lag behind in prompt fidelity. In contrast, VLM3D more effectively captures object interactions—rendering actions like “using a laptop”—and accurately models rare concepts such as “kaleidoscope” and “detective’s outfit.” It also excels at complex multi-object scenes, as shown by the jazz concert example with multiple instruments, including “a saxophone, a violin, and a drum”.

### 5.2. VLM Guidance for Feed-Forward Model

For this paradigm, we build upon the open-source pipeline of Hunyuan3D 2.0 [12, 51]. We apply our VLM3D reward (us-

Table 1. **Quantitative Results on 110 Prompts from the GPTEval3D Benchmark [44].** We compute all six GPTEval3D metrics—text alignment, 3D plausibility, texture–geometry coherence, geometry details, texture details, and overall score—to comprehensively evaluate 3D generation quality. VLM3D achieves the highest score on every metric, demonstrating its superior performance.

Method	Prompts from GPTEval3D					
	Alignment↑	Plausibility↑	T-G Coherency.↑	Geo Details↑	Tex Details↑	Overall↑
DreamFusion[26]	1000.0	1000.0	1000.0	1000.0	1000.0	1000.0
DreamGaussian[38]	1100.6	953.6	1158.6	1126.2	1130.8	951.4
Fantasia3D[7]	1067.9	891.9	1006.0	1109.3	1027.5	933.5
Instant3D[17]	1200.0	1087.6	1152.7	1152.0	1181.3	1097.8
Latent-NeRF[21]	1222.3	1144.8	1156.7	1180.5	1160.8	1178.7
Magic3D[19]	1152.3	1000.8	1084.4	1178.1	1084.6	961.7
ProlificDreamer[41]	1261.8	1058.7	1152.0	1246.4	1180.6	1012.5
MVDream[34]	1270.5	1147.5	1250.6	1324.9	1255.5	1097.7
DreamReward <sup>1</sup> [46]	1287.5	1195.0	1254.4	1295.5	1261.6	1193.3
DreamDPO[52]	1298.9	1171.9	1276.4	1373.2	1296.9	1203.1
VLM3D (Ours)	<b>1365.5</b>	<b>1293.7</b>	<b>1365.4</b>	<b>1419.0</b>	<b>1368.7</b>	<b>1268.6</b>

Table 2. **Quantitative Results for feed-forward pipelines.** VLM3D boosts both semantic and geometric quality.

Method	CLIP-D ↓	FID ↓	CLIP-FID ↓	Geo. ↓
CLAY [50]	0.22	310.3	53.11	0.63
Hunyuan3D [51]	0.23	338.6	54.01	0.58
VLM3D (Ours)	<b>0.19</b>	<b>274.9</b>	<b>45.79</b>	<b>0.49</b>

ing the same Qwen2.5-VL 7B backbone [2]) as a test-time guidance signal, as described in Sec. 4.3.2. This guidance is applied during the full 50 sampling steps of the Hunyuan3D shape generation pipeline (3D DiT [25]), steering the sampling of 3D latents. All experiments are run on a single NVIDIA A100 GPU with 60 seconds per 3D asset.

**Setup** To evaluate this test-time guidance, we use a suite of standard metrics including CLIP-D (text-shape alignment), FID and CLIP-FID (realism), and a comprehensive Geometry score on all cases shown in Fig. 1 and 4. We compare our VLM critic-based test-time guidance results directly against the original outputs of Hunyuan3D 2.1 [12] and CLAY [50].

**Quantitative Evaluation** We present quantitative results in Table 2. The VLM-guided generation process yields significant improvements across the board. The substantial gain in CLIP-D demonstrates that our  $r_{VLM}$  effectively steers the sampling process towards better text-semantic alignment. Furthermore, the improvement in the geometry scores confirms that our dual-query critic’s “Geometric Quality” check (Sec. 4.2) is crucial for fixing the spatial issues inherent in the original feed-forward generation.

**Qualitative Comparison** As shown in Fig. 1 and 4, our test-time guidance demonstrates a profound impact on spatial intelligence and part-assembly, a key weakness of SOTA feed-forward models [12, 50, 51]. For the prompt “a Navy sailor” the baseline Hunyuan3D generates a nonsensical collection of floating, disconnected parts. In stark contrast, our VLM3D-guided generation process, using the *exact same* feed-forward backbone, successfully assembles these components into a geometrically coherent object. Similarly, our VLM-based guidance correctly generates the full “leather glove” and the complete “glass window” with its frame, whereas the baselines produce incomplete or fractured geometry. This proves that our  $r_{VLM}$  can serve as an effective spatial critic to guide the DiT sampler away from incoherent states.

### 5.3. More Analyses and Ablation Studies

In this section, we dissect VLM3D’s behavior and quantify how key design choices affect 3D generation performance.

**Sensitivity to Prompt Perturbations** We assess VLM3D’s semantic fidelity on prompts that differ by a single concept. As shown in Fig. 5, we modify a farmer scene by changing the clothing color and specifying “chopping through a tree trunk.” VLM3D accurately reflects both the new color and the action, whereas MVDream fails to capture this detail action. Remarkably, VLM3D also exhibits superior spatial reasoning: when prompted to place a green apple “in” versus “beside” a plate, VLM3D honors each spatial relation, while MVDream fails. These results demonstrate VLM3D’s strong semantic alignment and its sensitivity to even subtle prompt variations.

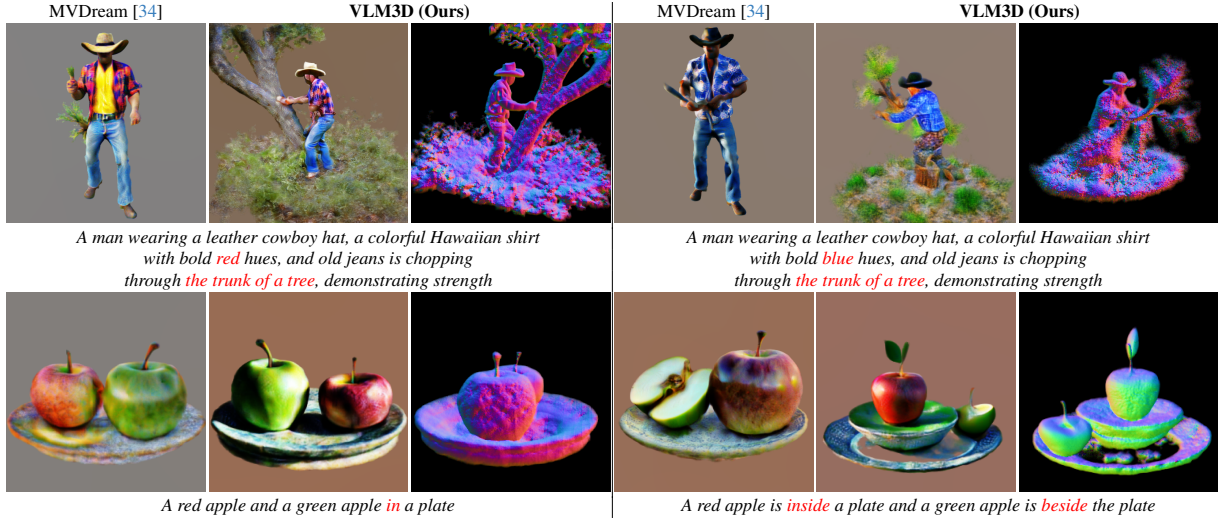


Figure 5. **Sensitivity Analysis to Text Perturbations.** We compare VLM3D and MVDream on pairs of prompts that differ by a single concept (highlighted in red). VLM3D accurately changes clothing color (first row), and updates spatial relations (second row), demonstrating its better semantic understanding than baselines.

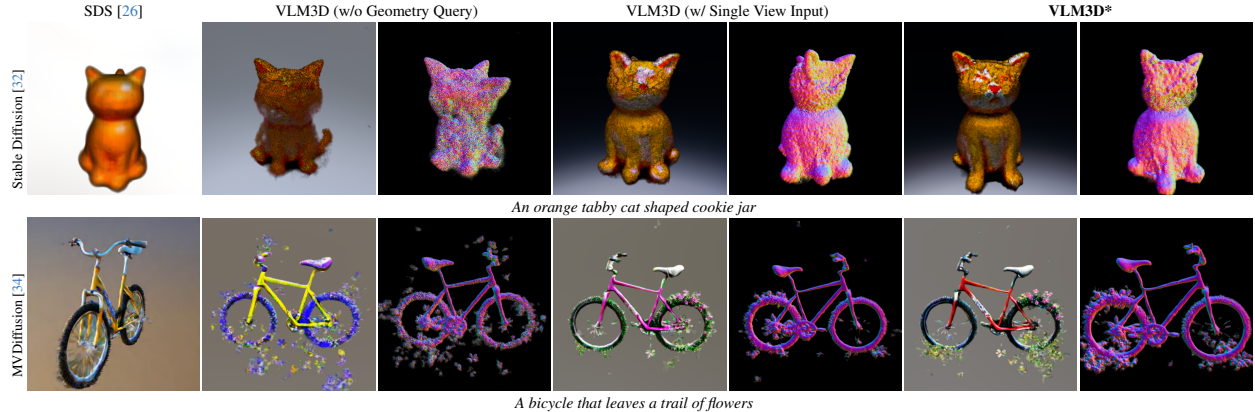


Figure 6. **Ablation of Geometric Query and Multi-View Input.** We assess the impact of (a) removing the explicit geometry-consistency query from the VLM prompt and (b) using a single view instead of multi-view images. Omitting either component degrades 3D quality—leading to Janus-face artifacts, floating parts, and fractured surfaces. Each row uses a different diffusion backbone: the top employs Stable Diffusion 2-1 [32], while the bottom uses MVDream [34].

**Ablation: Geometric Query in VLM Prompt** We assess the effect of explicitly querying geometric consistency in the VLM prompt. Without this query, VLM3D exhibits classic multi-face (Janus) artifacts on a cat prompt, and generates bicycles with floating parts and fractured surfaces (Fig. 6). Including the geometric query substantially mitigates these errors, confirming that explicit geometric guidance is critical.

**Ablation: Multi-View vs. Single-View Inputs** We further assess whether querying the VLM with multiple views is necessary for spatial coherence. When the VLM receives only a single rendered image instead of the full view set, VLM3D again suffers from Janus artifacts (Fig. 6). Multi-view inputs are critical to enforcing 3D consistency.

## 6. Conclusion

In this paper, we presented VLM3D, a novel framework that establishes large VLMs as general, differentiable semantic-and-spatial critic for text-to-3D generation. By introducing a dual-query reward—one for content fidelity and one for geometric constraints—and an end-to-end differentiable pipeline that backpropagates VLM log-odds, VLM3D achieves precise prompt alignment, mitigates view-consistency artifacts, and produces high-fidelity textures and geometry. We validate this in both SDS and native 3D generation paradigms.

**Limitations and Future Directions** Despite these advances, our VLM reward formulation can still struggle with very long or highly detailed prompts. For instance (Fig. 1), when tasked with generating the renowned ‘Embracing

Peace” statue, VLM3D correctly reproduces the kissing pose and dual figures—outperforming MVDream, which omits the nurse entirely—but still misses finer details such as the nurse’s lifted leg and outstretched arm. Interestingly, a standalone VLM can readily describe these details from a photograph, indicating that our current reward formulation does not fully leverage the VLM’s rich visual reasoning.

Building on these insights, we see several promising paths forward. First, disentangling semantic and geometric feedback—perhaps via separate VLM heads for content and geometry queries—might provide finer control over prompt fidelity and 3D consistency. Second, advanced query engineering, such as hierarchical or detail-focused cues, could ensure the VLM reward faithfully captures nuanced attributes and fine-grained descriptions.

## References

[1] Jinze Bai, Shuai Bai, Shusheng Yang, Shijie Wang, Sinan Tan, Peng Wang, Junyang Lin, Chang Zhou, and Jingren Zhou. Qwen-vl: A frontier large vision-language model with versatile abilities. *arXiv preprint arXiv:2308.12966*, 2023.

[2] Shuai Bai, Keqin Chen, Xuejing Liu, Jialin Wang, Wenbin Ge, Sibo Song, Kai Dang, Peng Wang, Shijie Wang, Jun Tang, et al. Qwen2. 5-vl technical report. *arXiv preprint arXiv:2502.13923*, 2025.

[3] Shuai Bai et al. Qwen2.5-vl technical report. *arXiv preprint arXiv:2502.13923*, 2025. Details Qwen2.5-VL architecture and capabilities.

[4] Weimin Bai, Siyi Chen, Wenzheng Chen, and He Sun. Blind inversion using latent diffusion priors. *arXiv preprint arXiv:2407.01027*, 2024.

[5] Hangbo Bao, Li Dong, Songhao Piao, and Furu Wei. Beit: Bert pre-training of image transformers. *arXiv preprint arXiv:2106.08254*, 2021.

[6] Boyuan Chen et al. Spatialvlm: Endowing vision–language models with spatial reasoning capabilities. In *CVPR*, 2024.

[7] Rui Chen, Yongwei Chen, Ningxin Jiao, and Kui Jia. Fantasia3d: Disentangling geometry and appearance for high-quality text-to-3d content creation. In *ICCV*, pages 22246–22256, 2023.

[8] An-Chieh Cheng et al. Spatialrgpt: Grounded spatial reasoning in vision–language models. In *arXiv preprint arXiv:2406.01584*, 2024.

[9] Jonathan Ho, Ajay Jain, and Pieter Abbeel. Denoising diffusion probabilistic models. In *NeurIPS*, pages 6840–6851, 2020.

[10] Susung Hong, Donghoon Ahn, and Seungryong Kim. Debiasing scores and prompts of 2d diffusion for robust text-to-3d generation. *arXiv preprint arXiv:2303.15413*, 2023.

[11] Yicong Hong, Kai Zhang, Jixiang Gu, Sai Bi, Yang Zhou, Difan Liu, Feng Liu, Kalyan Sunkavalli, Trung Bui, and Hao Tan. Lrm: Large reconstruction model for single image to 3d. *arXiv preprint arXiv:2311.04400*, 2023.

[12] Team Hunyuan3D, Shuhui Yang, Mingxin Yang, Yifei Feng, Xin Huang, Sheng Zhang, Zebin He, Di Luo, Haolin Liu, Yunfei Zhao, et al. Hunyuan3d 2.1: From images to high-fidelity 3d assets with production-ready pbr material. *arXiv preprint arXiv:2506.15442*, 2025.

[13] Chao Jia, Yinfai Yang, Ye Xia, Yi-Ting Chen, Zarana Parekh, Hieu Pham, Quoc Le, Yun-Hsuan Sung, Zhen Li, and Tom Duerig. Scaling up visual and vision-language representation learning with noisy text supervision. In *International conference on machine learning*, pages 4904–4916. PMLR, 2021.

[14] Bernhard Kerbl, Georgios Kopanas, Thomas Leimkühler, and George Drettakis. 3d gaussian splatting for real-time radiance field rendering. *ACM Transactions on Graphics*, 2023.

[15] Charles Laroche, Andrés Almansa, and Eva Coupete. Fast diffusion em: a diffusion model for blind inverse problems with application to deconvolution. In *Proceedings of the IEEE/CVF Winter Conference on Applications of Computer Vision*, pages 5271–5281, 2024.

[16] Junnan Li, Dongxu Li, Silvio Savarese, and Steven Hoi. Blip-2: Bootstrapping language-image pre-training with frozen image encoders and large language models. In *International conference on machine learning*, pages 19730–19742. PMLR, 2023.

[17] Jiahao Li, Hao Tan, Kai Zhang, Zexiang Xu, Fujun Luan, Yinghao Xu, Yicong Hong, Kalyan Sunkavalli, Greg Shakhnarovich, and Sai Bi. Instant3d: Fast text-to-3d with sparse-view generation and large reconstruction model. *arXiv preprint arXiv:2311.06214*, 2023.

[18] Siting Li, Pang Wei Koh, and Simon Shaolei Du. On erroneous agreements of clip image embeddings. *arXiv preprint arXiv:2411.05195*, 2024.

[19] Chen-Hsuan Lin, Jun Gao, Luming Tang, Towaki Takikawa, Xiaohui Zeng, Xun Huang, Karsten Kreis, Sanja Fidler, Ming-Yu Liu, and Tsung-Yi Lin. Magic3d: High-resolution text-to-3d content creation. In *CVPR*, pages 300–309, 2023.

[20] Haotian Liu, Chunyuan Li, Qingyang Wu, and Yong Jae Lee. Visual instruction tuning. *Advances in neural information processing systems*, 36:34892–34916, 2023.

[21] Gal Metzer, Elad Richardson, Or Patashnik, Raja Giryes, and Daniel Cohen-Or. Latent-nerf for shape-guided generation of 3d shapes and textures. *arXiv preprint arXiv:2211.07600*, 2022.

[22] Ben Mildenhall, Pratul P. Srinivasan, Matthew Tancik, Jonathan T. Barron, Ravi Ramamoorthi, and Ren Ng. Nerf: Representing scenes as neural radiance fields for view synthesis. In *ECCV*, 2020.

[23] Utkarsh Nath, Rajeev Goel, Eun Som Jeon, Changhoon Kim, Kyle Min, Yezhou Yang, Yingzhen Yang, and Pavan Turaga. Deep geometric moments promote shape consistency in text-to-3d generation. In *2025 IEEE/CVF Winter Conference on Applications of Computer Vision (WACV)*, pages 4331–4341. IEEE, 2025.

[24] Maitreya Patel, Naga Sai Abhiram Kusumba, Sheng Cheng, Changhoon Kim, Tejas Gokhale, Chitta Baral, et al. Triplet-clip: Improving compositional reasoning of clip via synthetic vision-language negatives. *Advances in neural information processing systems*, 37:32731–32760, 2024.

[25] William Peebles and Saining Xie. Scalable diffusion models with transformers. In *ICCV*, pages 4195–4205, 2023.

[26] Ben Poole, Ajay Jain, Jonathan T. Barron, and Ben Mildenhall. Dreamfusion: Text-to-3d using 2d diffusion. In *ICLR*, 2023. Introduces Score Distillation Sampling (SDS).

[27] Congpei Qiu, Yanhao Wu, Wei Ke, Xiuxiu Bai, and Tong Zhang. Refining clip’s spatial awareness: A visual-centric perspective. *arXiv preprint arXiv:2504.02328*, 2025.

[28] Alec Radford, Jong Wook Kim, Chris Hallacy, Aditya Ramesh, Gabriel Goh, Sandhini Agarwal, Girish Sastry, Amanda Askell, Pamela Mishkin, Jack Clark, et al. Learning transferable visual models from natural language supervision. In *International conference on machine learning*, pages 8748–8763. PMLR, 2021.

[29] Alec Radford et al. Learning transferable visual models from natural language supervision. *arXiv preprint arXiv:2103.00020*, 2021.

[30] Colin Raffel, Noam Shazeer, Adam Roberts, Katherine Lee, Sharan Narang, Michael Matena, Yanqi Zhou, Wei Li, and Peter J Liu. Exploring the limits of transfer learning with a unified text-to-text transformer. *Journal of machine learning research*, 21(140):1–67, 2020.

[31] Aditya Ramesh, Mikhail Pavlov, Gabriel Goh, Scott Gray, Chelsea Voss, Alec Radford, Mark Chen, and Ilya Sutskever. Zero-shot text-to-image generation. In *International Conference on Machine Learning*, pages 8821–8831. PMLR, 2021.

[32] Robin Rombach, Andreas Blattmann, Dominik Lorenz, Patrick Esser, and Björn Ommer. High-resolution image synthesis with latent diffusion models. In *Proceedings of the IEEE/CVF conference on computer vision and pattern recognition*, pages 10684–10695, 2022.

[33] Junyoung Seo, Susung Hong, Wooseok Jang, Inès Hyeonsu Kim, Minseop Kwak, Doyup Lee, and Seungryong Kim. Retrieval-augmented score distillation for text-to-3d generation. *arXiv preprint arXiv:2402.02972*, 2024.

[34] Yichun Shi, Peng Wang, Jianglong Ye, Mai Long, Kejie Li, and Xiao Yang. Mvdream: Multi-view diffusion for 3d generation. *arXiv preprint arXiv:2308.16512*, 2023.

[35] Jascha Sohl-Dickstein, Eric Weiss, Niru Maheswaranathan, and Surya Ganguli. Deep unsupervised learning using nonequilibrium thermodynamics. In *International conference on machine learning*, pages 2256–2265. pmlr, 2015.

[36] Yang Song, Jascha Sohl-Dickstein, Diederik P Kingma, Abhishek Kumar, Stefano Ermon, and Ben Poole. Score-based generative modeling through stochastic differential equations. *arXiv preprint arXiv:2011.13456*, 2020.

[37] Zhiqing Sun, Sheng Shen, Shengcao Cao, Haotian Liu, Chunyuan Li, Yikang Shen, Chuang Gan, Liang-Yan Gui, Yu-Xiong Wang, Yiming Yang, Kurt Keutzer, and Trevor Darrell. Aligning large multimodal models with factually augmented rlhf. *arXiv:2309.14525*, 2023.

[38] Jiaxiang Tang, Jiawei Ren, Hang Zhou, Ziwei Liu, and Gang Zeng. Dreamgaussian: Generative gaussian splatting for efficient 3d content creation. *arXiv preprint arXiv:2309.16653*, 2023.

[39] Feng Wang, Jieru Mei, and Alan Yuille. Sclip: Rethinking self-attention for dense vision-language inference. In *European Conference on Computer Vision*, pages 315–332. Springer, 2024.

[40] Peng Wang, Shuai Bai, Sinan Tan, Shijie Wang, Zhihao Fan, Jinze Bai, Keqin Chen, Xuejing Liu, Jialin Wang, Wenbin Ge, et al. Qwen2-vl: Enhancing vision-language model’s perception of the world at any resolution. *arXiv preprint arXiv:2409.12191*, 2024.

[41] Zhengyi Wang, Cheng Lu, Yikai Wang, Fan Bao, Chongxuan Li, Hang Su, and Jun Zhu. Prolificdreamer: High-fidelity and diverse text-to-3d generation with variational score distillation. *arXiv preprint arXiv:2305.16213*, 2023.

[42] Zecheng Wang et al. Taming mode collapse in score distillation for text-to-3d generation. In *CVPR*, 2024. Analyzes geometric inconsistency (“Janus problem”) in SDS.

[43] Tong Wu, Guandao Yang, Zhibing Li, Kai Zhang, Ziwei Liu, Leonidas Guibas, Dahua Lin, and Gordon Wetzstein. Gpt-4v(ision) is a human-aligned evaluator for text-to-3d generation. In *CVPR*, 2024.

[44] Tong Wu, Guandao Yang, Zhibing Li, Kai Zhang, Ziwei Liu, Leonidas Guibas, Dahua Lin, and Gordon Wetzstein. Gpt-4v (ision) is a human-aligned evaluator for text-to-3d generation. In *CVPR*, pages 22227–22238, 2024.

[45] Yinghao Xu, Zifan Shi, Wang Yifan, Hansheng Chen, Ceyuan Yang, Sida Peng, Yujun Shen, and Gordon Wetzstein. Grm: Large gaussian reconstruction model for efficient 3d reconstruction and generation. In *European Conference on Computer Vision*, pages 1–20. Springer, 2024.

[46] Junliang Ye, Fangfu Liu, Qixiu Li, Zhengyi Wang, Yikai Wang, Xinzhou Wang, Yueqi Duan, and Jun Zhu. Dreamreward: Text-to-3d generation with human preference. In *European Conference on Computer Vision*, pages 259–276. Springer, 2024.

[47] Jiahui Yu, Zirui Wang, Vijay Vasudevan, Legg Yeung, Mojtaba Seyedhosseini, and Yonghui Wu. Coca: Contrastive captioners are image-text foundation models. *arXiv preprint arXiv:2205.01917*, 2022.

[48] Arman Zarei, Keivan Rezaei, Samyadeep Basu, Mehrdad Saberi, Mazda Moayeri, Priyatham Kattakinda, and Soheil Feizi. Understanding and mitigating compositional issues in text-to-image generative models. *arXiv preprint arXiv:2406.07844*, 2024.

[49] Jiahui Zhang, Yurui Chen, Yanpeng Zhou, Yueming Xu, Ze Huang, Jilin Mei, Junhui Chen, Yu-Jie Yuan, Xinyue Cai, Guowei Huang, et al. From flatland to space: Teaching vision-language models to perceive and reason in 3d. *arXiv preprint arXiv:2503.22976*, 2025.

[50] Longwen Zhang, Ziyu Wang, Qixuan Zhang, Qiwei Qiu, Anqi Pang, Haoran Jiang, Wei Yang, Lan Xu, and Jingyi Yu. Clay: A controllable large-scale generative model for creating high-quality 3d assets. *ACM Transactions on Graphics (TOG)*, 43(4):1–20, 2024.

[51] Zibo Zhao, Zeqiang Lai, Qingxiang Lin, Yunfei Zhao, Haolin Liu, Shuhui Yang, Yifei Feng, Mingxin Yang, Sheng Zhang, Xianghui Yang, et al. Hunyuan3d 2.0: Scaling diffusion models for high resolution textured 3d assets generation. *arXiv preprint arXiv:2501.12202*, 2025.

[52] Zhenglin Zhou, Xiaobo Xia, Fan Ma, Hehe Fan, Yi Yang, and Tat-Seng Chua. Dreamdpo: Aligning text-to-3d generation with human preferences via direct preference optimization. *arXiv preprint arXiv:2502.04370*, 2025.

[53] Deyao Zhu, Jun Chen, Xiaoqian Shen, Xiang Li, and Mohamed Elhoseiny. Minigpt-4: Enhancing vision-language understanding with advanced large language models. *arXiv preprint arXiv:2304.10592*, 2023.